Elastic reflection FWI for subsalt velocity reconstruction: benchmark test with massive salt body

Qiang Guo and Christian Rivera*[†]
**King Abdullah University of Science & Technology (KAUST),* [†]*TOTAL E&P*

SUMMARY

Seismic imaging of the subsalt medium often contains invaluable information that can help locate the reservoir. However, a clear subsalt image highly relies on the accuracy of salt-body and subsalt velocity inversion, because both of them bear the kinematic information of seismic image at such a depth. Full waveform inversion (FWI) is a power technique that can enhance our ability of salt scenario interpretation, inspired by several successful applications. To achieve the goal of reliable salt-body/subsalt velocity inversion, we need to obtain not only a high-resolution interpretation of the salt structure, but also the low-to-medium wavenumbers of the velocity that is crucial to mitigate the notorious cycle-skipping issue. In this work we propose a reflection full waveform inversion (RFWI) workflow to improve the subsalt image. Instead of making FWI play the role of correcting for salt misinterpretation among some latest work, we are focused on implementing RFWI to the subsalt velocity building by making use of its ability of retrieving low-wavenumber model update along reflection wavepath. We introduce a RFWI workflow with a simultaneous optimization over the model perturbations and the low-wavenumber components, using a mixed scheme of objective function. A streamer dataset based on the benchmark model with massive salt body is used to validate our inversion strategy. We assume a reasonable interpretation of the salt geometry has been proceeded prior to our inversion, while there is little knowledge of the subsalt zone. In the situation of missing frequencies below 2 Hz and a limited offset-to-depth ratio below one, our RFWI workflow provides promising improvement in the subsalt imaging.

INTRODUCTION

In seismic exploration, to obtain a clear image of the subsalt reservoir is an extremely complex task. It is not only because of the challenge embedded in salt geometry/velocity estimation, but also the yet-to-be-developed velcity model building for the subsalt sediment Chen et al. (2018). The high-contrast salt boundary and the near-salt structures significantly increase the difficulty of velocity estimation, of which the study has long been a focus in seismic community. Full waveform inversion (FWI) is a technique developed to eliminate our historic practice of separating the propagation and scattering parts of the velocity model and produce a high-resolution delineation of the earth's subsurface medium Tarantola (1984). FWI is capable of handling the complex wave propagation around the salt body, so as lately it has been applied to the salt scenario (Huang et al., 2012; Zhang et al., 2017; Shen et al., 2018). It provides an automatic optimization of the model parameters by measuring an objective function in the data domain, which makes it more meaningful in some traditionally labor-intensive applications, still, to fully deploy FWI to the salt interpretation a serie of practical issues need to be addressed. More recently, Zhang et al. (2018) implemented FWI to correct the salt misinterpretation and proved it can effectively improve the subsalt image. In their work, a measurement of the cost function using traveltime information is devised to address the issue of amplitude discrepancy, which has been commonly regarded as one of the main practical issues that causes failure of FWI.

For a complete subsalt inversion, after we estimate the top geometry of the salt, usually a salt-flood inversion can be implemented to initially build the salt base. However, if no further information provided, a poor guess of the subsalt sediment velocity remains a serious impact to the image quality of subsalt reservoir. Encouraged by the successful, though limited, applications of FWI on salt structure delineation, we aim at developing a workflow in FWI framework to solve the velocity of subsalt sediment, which could follow the salt flood. The currently developed FWI methods based on refraction wave has been successfully implemented in building a high-resolution model for the shallow zone of the subsurface medium (Pratt, 1999; Choi and Alkhalifah, 2015). However, the practical issues like low frequencies cutoff and limited acquisition aperture hinder its abilities of estimating the deep model. To take advantage of the reflections that dominate the inversion of subsalt zone, a reliable estimation of the kinematics information of the model is usually required by the regular FWI approaches, in order to achieve a natural transition from the low-wavenumber velocity to a high-resolution output (Mora, 1989; Alkhalifah and Wu, 2017; Symes, 2008; Rivera* et al., 2015; Feng and T. Schuster, 2018). Xu et al. (2012), based on the work of Chavent and Clément (1993); Plessix et al. (1995); Clément et al. (2001), suggested a waveform-based velocity building workflow using the reflections generated by a migration/demigration process, referred to as RFWI. RFWI has shown considerable effectiveness and robustness in some recent studies (Guo and Alkhalifah, 2017; Rivera et al., 2018; Guo et al., 2017) and, moreover, it has been implemented to deal with the interpretation of the salt scenario (Chen et al., 2018), and established its role in guiding the dirty salts and near-salt sediment velocity inversion.

In this work, we will demonstrate how RFWI can be used to produce a high-resolution velocity model starting from little knowledge of the subsalt medium. Our workflow is applied, in both acoustic and elastic courses, to a 2D streamer benchmark dataset from a field with massive salt body. In this example, the target region is overlaid by a mostly homogeneous salt with huge thickness. We assume an reasonable interpretation of the salt body has been proceeded, e.g., by salt flood. To mimic the practical situation, we adopt an acquisition with limited offset (maximum of 12 km, to-depth ratio less than one) and mute the frequency components below 2 Hz. In such case, the FWI implementation focused on diving wave will fail to illuminate the subsalt, thus the reflections become the only information to rely on. We apply a simultaneous optimization over the model perturbations (image) and the low-wavenumber velocity, which controls the kinematics of the wave propagation. The estimated subsalt velocity through this workflow produces obvious improvement to the subsalt migration. Including the inverted model perturbation into the velocity results in a high-resolution image of the subsalt sediment that matches the true answer. The inversion based on acoustic approximation is not an ideal solution to the subsalt inversion, while it performs a plausible initial velocity building for sequential elastic inversion.

REFLECTION WAVEFORM INVERSION

The general form of the objective function used in our optimization can be expressed as

$$\min\ E = \frac{1}{2}\sum_{s,r}\int dt\ \|\mathbf{A}[u(s,\mathbf{x},t;c_0)+\tilde{u}(s,\mathbf{x},t;c_0,\mathbf{I})]-d(s,r,t)\|^2, \tag{1}$$

which is formulated by Alkhalifah and Wu (2016); Wu and Alkhalifah (2015), based on previous finding of Albertin et al. (2013). Virieux et al. (2015) also proposed a similar objective function, but with a measurement split into two terms. $u(s,\mathbf{x},t;c_0)$ is the source wavefield modeled using the smoothed background model; the wavefield $\tilde{u}(s,\mathbf{x},t;c_0,\mathbf{I})$ is the first-order scattering of Born series, which can be calculated by the migration and demigration process:

$$\mathbf{F}\left[c_0\right]\tilde{u}(s,\mathbf{x},t) = \int d\mathbf{x}\int d\mathbf{x}_s\,\nabla u(s,\mathbf{x},t)\times\mathbf{I}(\mathbf{x}_s)\delta(\mathbf{x}-\mathbf{x}_s), \tag{2}$$

where $\mathbf{F}\left[c_0\right]$ is the wave equation operator. By producing reflections from the demigration process instead of the velocity model itself, we can retrieve the low-wavenumber model update along the reflection wavepath, without inducing the scattering information into the velocity inversion. The gradient of this objective used to update the velocity can be expressed as

$$\begin{aligned}\frac{\partial E}{\partial c_0(\mathbf{x})} \quad &= \quad -\sum_s\frac{1}{c}\int dt\ \left[\nabla^2 u(s,\mathbf{x},t)\mu(s,\mathbf{x},t)\right.\\ &+ \quad \left.\nabla^2\tilde{u}(s,\mathbf{x},t)\mu(s,\mathbf{x},t) + \nabla^2 u(s,\mathbf{x},t)\tilde{\mu}(s,\mathbf{x},t)\ \right],\end{aligned} \tag{3}$$

where μ and $\tilde{\mu}$ are the adjoint wavefield calculated with the background medium and the one scattered at the image. Since we include both the wave propagation in the smoothed model and the scattering one in one objective function, the gradient actually consists of the update along the reflection wavepath as well as the diving wavepath.

We develop a workflow of inverting for the subsalt velocity using RFWI, which is shown in Table 1. RFWI can be implemented either in time or frequency domain (Wang et al., 2013; Wu and Alkhalifah, 2014), but the one thing in common between these implementations is that the property of demigrated reflections are highly sensitive to the image quality. In order to achieve an optimal fit of the data, a true amplitude migration is required, which can be achieved with a least-squares optimization.

As we do a simultaneous inversion for the model perturbations and the low-wavenumber velocity, we suggest a more flexible strategy in choosing the cost function depending on the decoupled features of these two components (Guo and Alkhalifah, 2017). For the inversion of model perturbations, we suggest using the $l2$-norm misfit function to guarantee a wise data match of the reflectivities at the near-zero offsets. For the slowly varying background model, which mainly influences the kinematic features of reflection/transmission, we suggested using the normalized cross-correlation objective function (Choi and Alkhalifah, 2012) to mitigate the amplitude effects. Even though the acoustic approximation is adopted to invert for the elastic data, its sensitivity with respect to the amplitude becomes relatively trivial as we are focused to the kinematics information. As the subsalt zone is dominated by the reflections, we formulate our correlation-based objective function using the demigrated data $\tilde{u}$ and the recorded reflection data d_r, from which the diving wave calculated by the initial model is subtracted, corresponding to equation 1.

$$\min\ E_{corr_0} = -\sum_{s,r}\int dt\ \frac{\tilde{u}(s,\mathbf{x}_r,t)}{\|\tilde{u}(s,\mathbf{x}_r,t)\|}\frac{d_r(s,\mathbf{x}_r,t)}{\|d_r(s,\mathbf{x}_r,t)\|}. \tag{4}$$

2D STREAMER BENCHMARK WITH MASSIVE SALT

We apply our proposed RFWI workflow to a streamer benchmark dataset of massive salt body (thickness over 5 km). Figure 1 shows the subsalt zone of the true elastic model. The scale of subsalt sediment shown is 7 km from top to bottom. The density is also included, which was built with wells and extrapolated using existing seismic reflectivity. We generate the shear wave velocity based on Castagna et al. (2005) in the sediments, and using constant values in the salt body.

We use the Ricker's wavelet with a peak frequency of 8 Hz as our source function, and filter out the frequencies below 2 Hz to imitate practical conditions. We start with an initial P-wave velocity model shown in Figure 2. The velocity of zone right below the salt is set to be a constant that is far from the true answer. By doing so, we can verify the robustness of RFWI in

Table 1: Our suggested RFWI workflow for the subsalt inversion

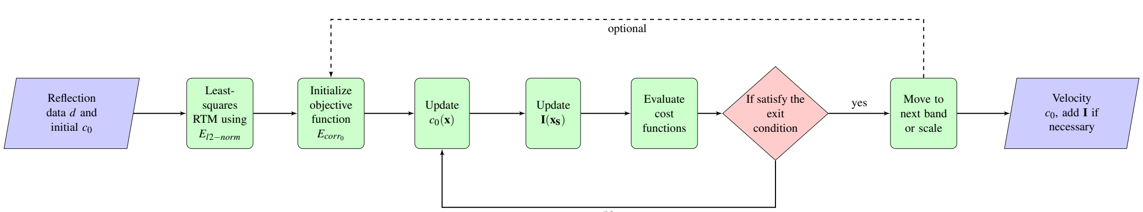

dealing with such a case that no priori information is available under the salt. As we can see in Figure 3a, the gradient of P-wave velocity calculated using elastic FWI fails to provide any low-wavenumber information below the salt.

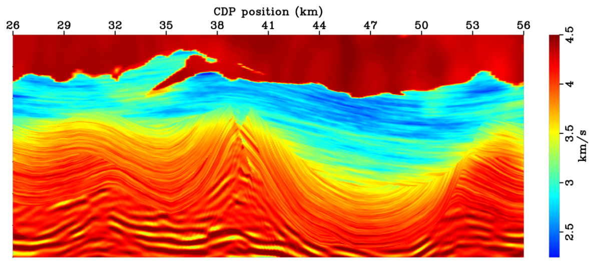

(a)

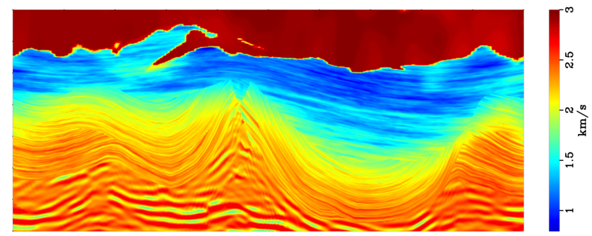

(b)

Figure 1: The subsalt sediment of true model: (a) P-wave velocity, (b) S-wave velocity. The density was built with wells and extrapolated using existing seismic reflectivity. The subsalt zone is 7 km in size from top to bottom.

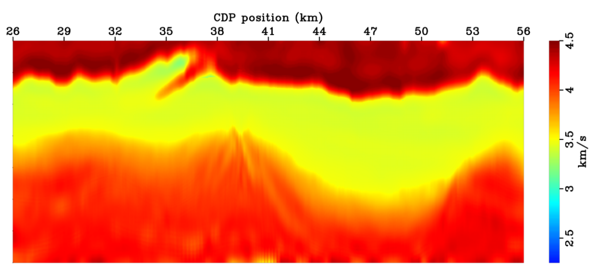

Figure 2: The initial P-wave velocity model.

First, we apply our RFWI based on the acoustic approximation, where the amplitude mismatch is supposed to be handled by the correlation-based objective function. The gradient along the reflection wavepath providing a reasonably low-wavenumber update of the background model, which is shown in Figure 3b. After each iteration of velocity update, we measure the objective function and switch to the image update. We run three stage of inversion. After the first stage of optimization, we apply a smoothing with larger window size and reduce the smoothing window as we move to the next stage. Figure 4 shows the velocity after the acoustic inversion.

Three velocity profiles of the subsalt zone, located at x= 41.5km, 45.7km and 48.5km are shown in Figure 5, which reveal the low wavenumbers of the P-wave velocity recovered through our optimization. The optimized image of the subsalt zone is shown in Figure 6b. Compared to the least-squares RTM calculated using the initial velocity (Figure 6a), the simultaneous

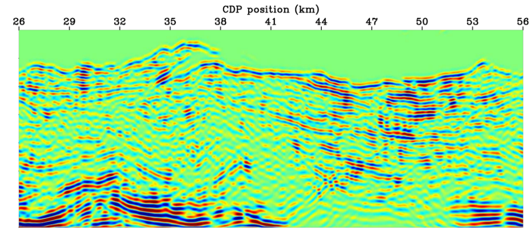

(a)

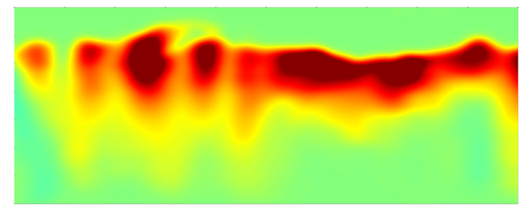

(b)

Figure 3: The gradient of regular elastic FWI (a) for P-wave velocity; (b) gradient calculcated from acoustic RFWI, using a smoothing window of 800m (in horizon) by 200m (in depth).

inversion results in an image with the improved resolution and accuracy. One part of image is used for comparison with the one calculated using the smoothed true velocity (shown in Figure 7b), which is supposed to give the accurate subsalt structure.

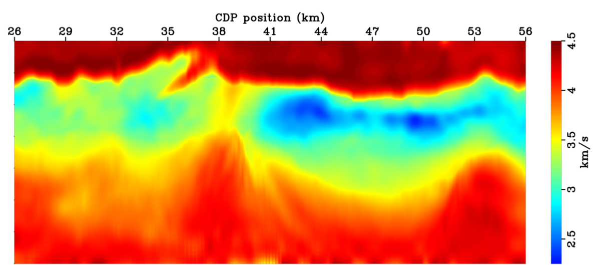

Figure 4: The inverted model after the last stage of the acoustic RFWI.

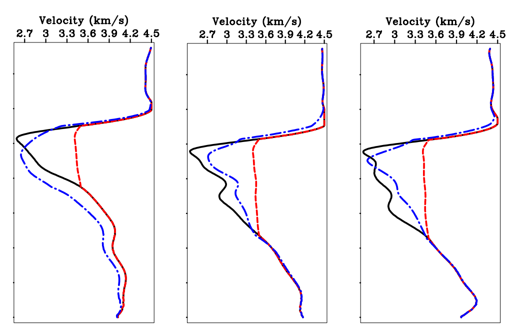

(a) (b) (c)

Figure 5: Three velocity profiles of subsalt zone, located at x=(a) 41.5 km, (b) 45.7 km and (c) 48.5 km. Inverted ones are in blue dot dash; initial in red dash; true answer in black.

Elastic Reflection Waveform Inversion

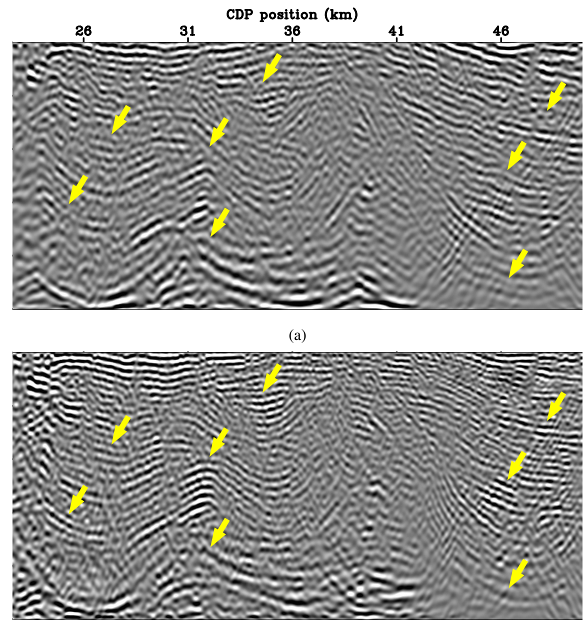

(a)

(b)

Figure 6: The least-squares RTM calculated using (a) the initial velocity and (b) the inverted velocity. The places where the resolution gets improved are marked by arrows.

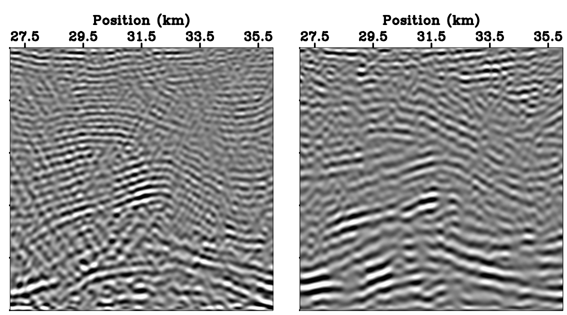

(a) (b)

Figure 7: The least-squares RTM of a subsalt zone calculated using (a) the inverted velocity and (b) the smoothed version of true velocity.

After we obtain a reasonable P-wave velocity for the subsalt zone, we move to the elastic inversion, which is expected to mitigate the artifacts caused by acoustic approximation and provide more details. For the elastic course, we still rely on RFWI based on the development of Guo and Alkhalifah (2017). We first estimate least-squares elastic RTM based on the concept of model perturbations (δV_p and δV_s) (Guo and Alkhalifah, 2017; Duan et al., 2017; Feng and Schuster, 2017). Using the same strategy of acoustic case, we implement a simultaneous inversion for the velocities and the model perturbations. Taking the elastic parameters into account enables us to better handle the dynamic effects of the dataset. Hence, the elastic inversion produces an image with improved resolution (show in Figure 8b), which is supposed to help the velocity estimation. The optimized model perturbations are added to the inverted velocity to form a high-resolution image of the subsalt sediment. The result containing the right zone of the subsalt is shown in Figure 9a.

DISCUSSIONS AND CONCLUSIONS

RFWI provides low-to-medium wavenumber velocity update, benefitting from the large scattering angle along wavepath. Under the challenging situation of limited offset and frequency band, our RFWI workflow builds a reasonably accurate subsalt velocity that provides a good stepping stone to FWI. The correlation-based objective function works properly with the acoustic approximation, still it is necessary to apply smoothing to guarantee a balanced update at the early stage.

ACKNOWLEDGMENTS

We thank TOTAL E&P for supporting this study, and B. Duquet, P. Williamson, F. Audebert, P. T. Trinh and X. Lu for helpful discussions and suggestions. The author, Qiang Guo, thanks KAUST for its support in developing elastic RWI.

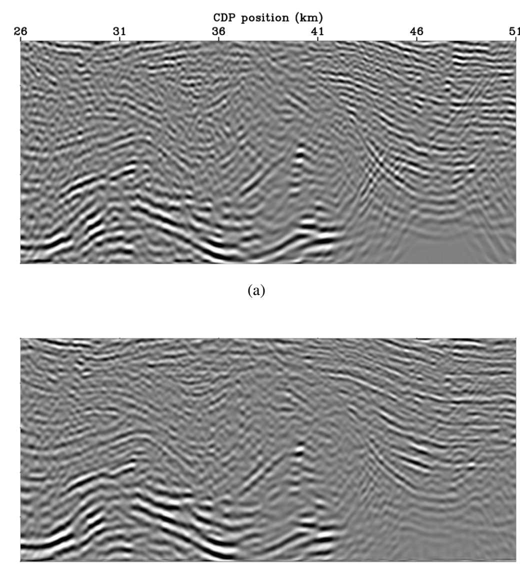

(a)

(b)

Figure 8: The least-squares acoustic RTM (a) versus least-squares elastic RTM (b) for δV_p.

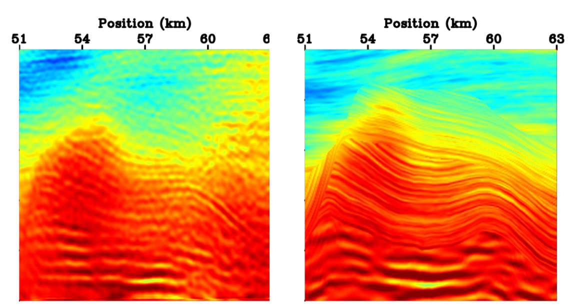

(a) (b)

Figure 9: Part of the optimized P-wave velocity model (a) of the subsalt zone with the model perturbations added to it and (b) the true answer.

REFERENCES

Albertin, U., G. Shan, and J. Washbourne, 2013, *in* Gradient orthogonalization in adjoint scattering-series inversion: 1058–1062.

Alkhalifah, T., and Z. Wu, 2016, The natural combination of full and image-based waveform inversion: Geophysical Prospecting, **64**, 19–30.

———, 2017, Migration velocity analysis using pre-stack wave fields: Geophysical Prospecting, **65**, 639–649.

Castagna, J. P., M. L. Batzle, and R. L. Eastwood, 2005, *in* Relationship between compressional and shearwave velocities in classic silicate rocks: 582–584.

Chavent, G., and F. Clément, 1993, Waveform inversion through MBTT formulation: Research Report RR-1839, INRIA. (Projet IDENT).

Chen, J., D. Sixta, G. Raney, V. Mount, E. Riddle, A. Nicholson, H. Ma, H. Ji, and C. Peng, 2018, *in* Improved subsalt imaging from reflection full-waveform inversion-guided salt scenario Interpretation: A case history from deepwater Gulf of Mexico: 3773–3777.

Choi, Y., and T. Alkhalifah, 2012, Application of multi-source waveform inversion to marine streamer data using the global correlation norm: Geophysical Prospecting, **60**, 748–758.

———, 2015, Unwrapped phase inversion with an exponential damping: Geophysics, **80**, R251–R264.

Clément, F., G. Chavent, and S. Gómez, 2001, Migration-based traveltime waveform inversion of 2-d simple structures: A synthetic example: GEOPHYSICS, **66**, 845–860.

Duan, Y., A. Guitton, and P. Sava, 2017, Elastic least-squares reverse time migration: GEOPHYSICS, **82**, 1–65.

Feng, S., and G. T. Schuster, 2018, Transmission + reflection anisotropic waveequation traveltime and waveform inversion: Geophysical Prospecting, **67**.

Feng, Z., and G. T. Schuster, 2017, Elasticleast-squares reverse time migration: Geophysics, **82**, S143–S157.

Guo, Q., and T. Alkhalifah, 2017, Elastic reflection-based waveform inversion with a nonlinear approach: GEOPHYSICS, **82**, R309–R321.

Guo, Q., T. A. Alkhalifah, and Z. Wu, 2017, Velocity building by reflection waveform inversion without cycle-skipping: Presented at the , EAGE Publications BV.

Huang, W., K. Jiao, D. Vigh, J. Kapoor, D. Watts, H. Li, D. Derharoutian, and X. Cheng, 2012, Application of full-waveform inversion for salt sediment inclusion inversion: SEG Technical Program Expanded Abstracts 2012, 1–5.

Mora, P., 1989, *in* Inversion=migration+tomography: Springer Berlin Heidelberg, 78–101.

Plessix, R., Y. D. Roeck, and G. Chavent, 1995, Automatic and simultaneous migration velocity analysis and waveform inversion of real data using a mbtt/wkb j formulation: 1099–1102.

Pratt, R. G., 1999, Seismic waveform inversion in the frequency domain, part 1: Theory and verification in a physical scale model: GEOPHYSICS, **64**, 888–901.

Rivera, C. A., E. Bergounioux, D. Ortiz-Rubio, and F. Audebert, 2018, Integrating reflection-fwi in depth imaging velocity model building workflows: 80th EAGE Conference & Exhibition 2018 Workshop Programme.

Rivera*, C. A., B. Duquet, and P. Williamson, 2015, *in* Laplace-Fourier FWI as an alternative model building tool for depth imaging studies: Application to marine carbonates field: 1054–1058.

Shen, X., I. Ahmed, A. Brenders, J. Dellinger, J. Etgen, and S. Michell, 2018, Full-waveform inversion: The next leap forward in subsalt imaging: The Leading Edge, **37**, 67b1–67b6.

Symes, W. W., 2008, Migration velocity analysis and waveform inversion: Geophysical Prospecting, **56**, 765–790.

Tarantola, A., 1984, Inversion of seismic reflection data in the acoustic approximation: Geophysics, **49**, 1259–1266.

Virieux, J., R. Brossier, W. Zhou, and S. Operto, 2015, Full waveform inversion of diving & reflected waves for velocity model building with impedance inversion based on scale separation: Geophysical Journal International, **202**, 1535–1554.

Wang, S., F. Chen, H. Zhang, and Y. Shen, 2013, Reflection-based full waveform inversion (rfwi) in the frequency domain: 83rd Annual International Meeting, SEG, Expanded Abstracts, 877–881.

Wu, Z., and T. Alkhalifah, 2014, Full waveform inversion based on the optimized gradient and its spectral implementation: 76th Conference & Exhibition, EAGE, Extended Abstracts.

———, 2015, Simultaneous inversion of the background velocity and the perturbation in full-waveform inversion: Geophysics, **80**, R317–R329.

Xu, S., D. Wang, F. Chen, Y. Zhang, and G. Lambare, 2012, Full waveform inversion for reflected seismic data: 74th Conference & Exhibition incorporating SPE EUROPEC, EAGE, Extended Abstracts.

Zhang, L., D. Vigh, X. Cheng, K. Jiao, and D. Sun, 2017, An application of full-waveform inversion with automated adjustment of salt geometry: SEG Technical Program Expanded Abstracts 2017, 1502–1506.

Zhang, Z., J. Mei, F. Lin, R. Huang, and P. Wang, 2018, *in* Correcting for salt misinterpretation with full-waveform inversion: 1143–1147.